nature cell biology

The planar cell polarity effector Fuz is essential for targeted membrane trafficking, ciliogenesis and mouse embryonic development

Ryan S. Gray[1], Philip B. Abitua[1,7], Bogdan J. Wlodarczyk[2,7], Heather L. Szabo-Rogers[4], Otis Blanchard[1], Insuk Lee[5,6], Greg S. Weiss[1,5], Karen J. Liu[4], Edward M. Marcotte[5], John B. Wallingford[1,8] and Richard H. Finnell[2,3,8]

The planar cell polarity (PCP) signalling pathway is essential for embryonic development because it governs diverse cellular behaviours, and 'core PCP' proteins, such as Dishevelled and Frizzled, have been extensively characterized[1–4]. By contrast, the 'PCP effector' proteins, such as Intu and Fuz, remain largely unstudied[5,6]. These proteins are essential for PCP signalling, but they have never been investigated in mammals and their cell biological activities remain entirely unknown. We report here that Fuz mutant mice show neural tube defects, skeletal dysmorphologies and Hedgehog signalling defects stemming from disrupted ciliogenesis. Using bioinformatics and imaging of an *in vivo* mucociliary epithelium, we established a central role for Fuz in membrane trafficking, showing that Fuz is essential for trafficking of cargo to basal bodies and to the apical tips of cilia. Fuz is also essential for exocytosis in secretory cells. Finally, we identified a Rab-related small GTPase as a Fuz interaction partner that is also essential for ciliogenesis and secretion. These results are significant because they provide new insights into the mechanisms by which developmental regulatory systems such as PCP signalling interface with fundamental cellular systems such as the vesicle trafficking machinery.

PCP signalling is essential for a variety of vertebrate developmental events, including morphogenesis of the neural tube, heart, kidney and ear. Components of the pathway govern a wide array of polarized cellular behaviours, including cell intercalation and migration, cell division, and ciliogenesis[1,2]. In *Drosophila melanogaster* and *Xenopus laevis*, the 'PCP effector' proteins, including Fuz, act together with 'core' components such as Dishevelled (Dvl)[5,6]. The PCP effectors have received little attention, being the subject of only a single study in vertebrate animals[6], whereas the core proteins have been the subject of intense study[1,2,7–9]. Fuz is essential for ciliogenesis in *Xenopus*[6], but its precise molecular function, as with all intracellular PCP proteins, remains very poorly understood.

We examined whether PCP effectors were essential for mammalian development by obtaining murine embryonic stem (ES) cells with a gene-trap inserted into the second of eleven exons in *Fuz*, the mouse orthologue of *Drosophila Fuzzy* and *Xenopus Fuz*. This gene trap is predicted to disrupt transcription of the *Fuz* gene. These cells were used to generate mice carrying the inactive *Fuz* allele. Litters from heterozygous matings produced very few viable full-term homozygous mutant pups, as the small litters did not follow the expected genotypic ratios upon analysis. Homozygous fetuses were obtained at embryonic day (E) 18.5, and these mice had a wide range of developmental defects (Fig. 1; Supplementary Information, Fig. S1).

All homozygous mutant mice had severe developmental defects, including craniofacial malformations and incompletely penetrant rostral neural tube closure defects, such as exencephaly and encephaloceles (Fig. 1b; Supplementary Information, Fig. S1d, e). Some *Fuz* mutant mice had normal neural tube closure despite having severe craniofacial and ocular defects (Supplementary Information, Fig. S1f). However, even mice with mild overt neural tube closure defects had severely dilated brain ventricles (Supplementary Information, Fig. S1h). *Fuz* mutant mice consistently showed polydactyly on all limbs (Fig. 1d), and we observed widespread defects in skeletal development and organogenesis, including malformed sternum, ribs and long bones, as well as severely hypoplastic lungs and conotruncal defects (Fig. 1c–f, i, j; Supplementary Information, Fig. S1i–l). This spectrum of defects reflects the phenotype of mice with defects in ciliogenesis[10,11], and is also reminiscent of the defects

[1]Dept. of Molecular Cell and Developmental Biology, Institute for Cellular and Molecular Biology, University of Texas, Austin, Texas 78712, USA. [2]Center for Environmental and Genetic Medicine, Institute of Biosciences and Technology, Texas A&M Health Science Center, Houston, Texas 77030, USA. [3]The Texas A&M Institute for Genomic Medicine, Houston, Texas 77030, USA. [4]Dept. of Craniofacial Development, King's College London, London, UK SE1 9RT. [5]Dept. of Chemistry and Biochemistry, Center for Systems and Synthetic Biology, Institute for Cellular and Molecular Biology, University of Texas, Austin, Texas 78712, USA. [6]Current address: Network Biotechnology Laboratory, Yonsei University, 134 Shinchon-dong, Seodaemun-gu, Seoul 120-749, South Korea.
[7]These authors contributed equally.
[8]Correspondence should be addressed to J.B.W. or R.H.F. (e-mail: wallingford@mail.utexas.edu; rfinnell@ibt.tamhsc.edu)

Received 25 March 2009; accepted 22 June 2009; published online 20 September 2009; DOI: 10.1038/ncb1966

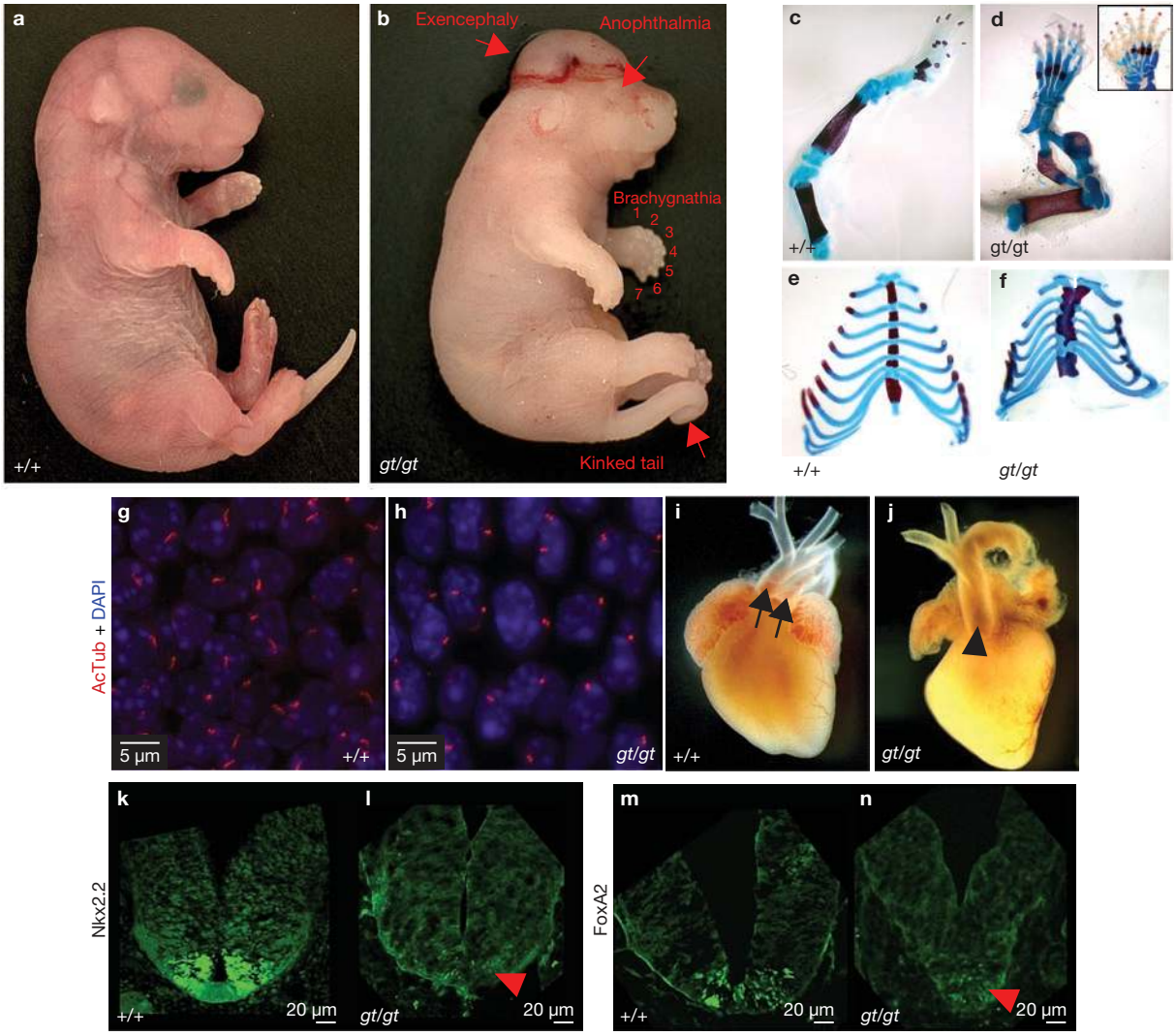

Figure 1 Mice lacking a functional *Fuz* gene have multiple developmental defects. (**a**) Wild-type (+/+) mouse, E18.5 and (**b**) $Fuz^{gt/gt}$ mouse. Skeletal preparation of (**c**) wild-type hindlimb and (**d**) $Fuz^{gt/gt}$ hindlimb. Inset shows a paw with extreme polydactyly from a $Fuz^{gt/gt}$ mouse. (**e**, **f**) Sternum preparations from wild-type and $Fuz^{gt/gt}$ mice. (**g**, **h**) Confocal projections of Meckels' cartilage stained with acetylated tubulin (red) and DAPI (blue) show diminished primary cilia in $Fuz^{gt/gt}$ mouse sections. Scale bars, 5 µm. Cilia length (mean ± s.e.m.) was 1.73 ± 0.06µm in wild-type ($n = 70$) and 0.87 ± 0.04 µm in $Fuz^{gt/gt}$ ($n = 52$) mice; $P < 0.001$. (**i**) Dissected heart from a wild-type mouse. Arrows indicate outflow tracts. (**j**) Dissected heart from a $Fuz^{gt/gt}$ mouse. Arrowhead indicates single outflow tract. (**k**, **l**) Expression of Nkx2.2 (green) in the ventral neural tube is diminished in $Fuz^{gt/gt}$ mice (red arrowhead). (**m**, **n**) Expression of FoxA2 (green) in the ventral neural tube is lost in $Fuz^{gt/gt}$ mice (red arrowhead).

in human patients with ciliopathic syndromes such as Bardet-Biedl Syndrome (BBS)[12,13], Meckel-Gruber syndrome[14] or Jeune's asphyxiating thoracic dystrophy[15].

Collectively, these malformations are consistent with a failure of cilia-mediated Hedgehog signalling in *Fuz* mutant mice, so we next examined the expression of Hedgehog target genes in the spinal cord[6,10]. We found that although Nkx2.2 and FoxA2 were robustly expressed in the ventral spinal cord of control mice, these expression domains were almost entirely absent in *Fuz* mutant mice (Fig. 1k–n). Finally, we found that *Fuz* mutant mice had defects in primary ciliogenesis. Immunostaining for acetylated tubulin revealed that primary cilia in the *Fuz* mutant mice were significantly shorter than cilia of wild-type mice (Fig. 1g–h). Despite the extremely significant difference in average length, the effect on cilia length was variable, and cilia of nearly normal length were occasionally observed in *Fuz* mutant mice (Supplementary Information, Fig. S1b), consistent with the result of *Fuz* knockdown in *Xenopus*[6]. This finding is also consistent with the *Fuz* mutant mouse embryonic phenotypes; *Fuz* mutants resemble single BBS mutations or hypomorphic alleles of IFT genes, in which cilia are present but defective[10,11]. By contrast, *Kif3a* null mice lack cilia entirely and show far more severe embryonic phenotypes[16].

In addition to these defects in Hedgehog signalling, *Fuz* mutant mice also showed defects consistent with a failure of PCP signalling. For example, the homozygous *Fuz* mutant mice had kinked or curly tails (Fig. 1b), a phenotype that is consistently associated with heterozygous mutations in core PCP proteins such as Dvl or Vangl2[8,9]. The homozygous *Fuz* mutant mice also had cardiac defects, including single outflow tracts and ventral septal defects (Fig. 1j; Supplementary Information, Fig. S1l), similar to those observed in mouse models lacking core PCP genes[2,8]. The pattern of congenital malformations

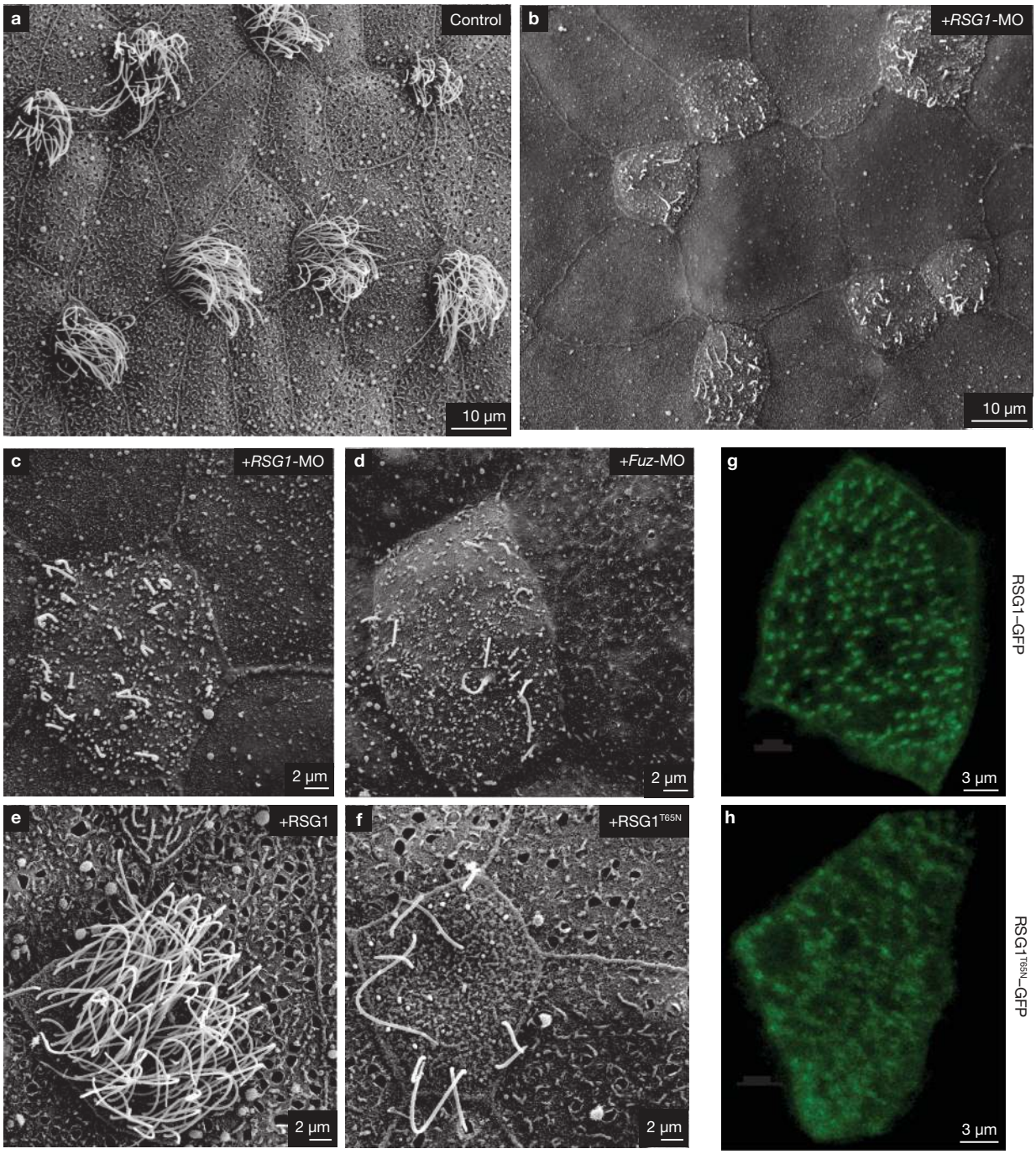

Figure 2 RSG1 controls ciliogenesis and secretion. (**a**) Scanning electron micrograph of intact, control *Xenopus* ciliated epidermis reveals multiciliated cells and surrounding mucous secreting cells. (**b**) RSG1 morphants show defects in ciliogenesis and absence of mucous granules and exocytic pits. (**c**) Higher-magnification view of RSG1 morphant ciliated epidermis showing diminished cilia numbers and lengths and a decrease in exocytic pits in neighbouring secretory cells. (**d**) Fuz morphants also show diminished cilia numbers and lengths and a decrease in exocytic pits in secretory cells. (**e**, **f**) Epidermal targeted overexpression of RSG1^{T65N}, but not wild-type RSG1, results in defects in ciliogenesis, as well as decreases in mucous granules and exocytic pits in secretory cells. (**g**, **h**) GFP–RSG1 (low-level expression) localizes to the basal body region of multiciliated cells, whereas GFP–RSG1^{T65N} (low-level expression) in multiciliated cells is diffuse and not tightly associated with basal bodies. Observations of fluorescence levels following expression of *GFP–RSG1* and *GFP–RSG1^{T65N}* mRNA were comparable, suggesting similar rates of translation for the two proteins.

in the Fuz mutant mice is thus entirely consistent with that found in *Xenopus* embryos following *Fuz* knockdown[6]. Fuz morphant *Xenopus* embryos and *Fuz* mutant mice each had comparatively mild PCP defects together with more severe defects in cilia-mediated developmental events.

The evolutionarily conserved role for Fuz from frogs to mammals provides us an opportunity to exploit the tremendous wealth of bioinformatics data in mammalian systems to help us elucidate the mechanisms of action for the Fuz protein. We first queried the human interactome for potential Fuz-interacting proteins. We noted that high-throughput

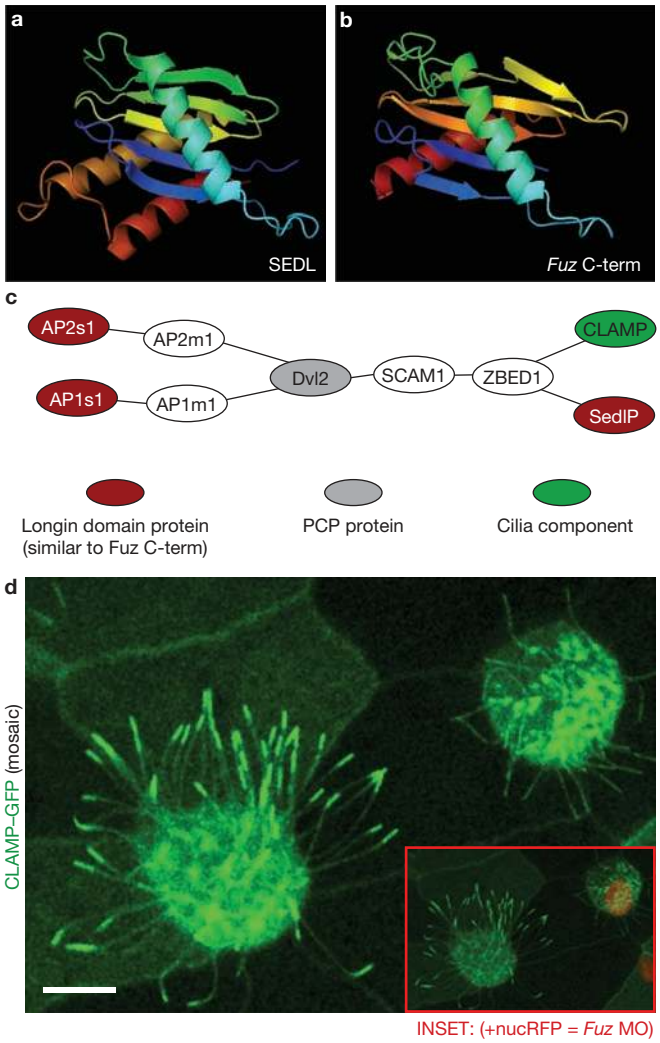

Figure 3 Homology modelling, network predictions and experimental validation suggest a trafficking function for Fuz. (**a, b**) Rendered protein models (Open-Source PyMOL 0.99rc6 software). (**a**) SedI N-terminal domain (pdb:1H3Q). (**b**) 1H3Q based homology threaded model of the C terminus (amino acids 287–419) of *Xenopus* Fuz protein. (**c**) Illustration of experimentally derived protein–protein interactions (see Supplementary Information Methods) linking Dvl2 with longin-domain proteins AP1s, AP2s and SedIP, as well as CLAMP. (**d**) Mosaic imaging of live embryo expressing CLAMP–GFP, which localizes to ciliary axonemes and apical tips. A nucRFP marks the nuclei, serving as a lineage tracer for co-injected Fuz MO. The confocal slice reveals a loss of apical localized CLAMP–GFP at ciliary tips in *Fuz* MO cells (inset shows merge of **d** and a more basal slice to display nucRFP signal). Scale bar, 10 μM (**d**).

yeast two-hybrid screening[17] suggested a weak interaction between human Fuz and the protein encoded by human chromosome 1 open reading frame 89 (Chr1orf89). BLAST predicted this gene to encode a small GTPase similar to REM2 and the vesicle-targeting Rab proteins (Supplementary Information, Fig. S2a). On the basis of this homology, we propose renaming C1orf89 to Rem/Rab–Similar GTPase 1 (RSG1). Co-immunoprecipitation confirmed that RSG1 associates with Fuz (Supplementary Information, Fig.S2b).

To assess the function of RSG1, we designed an antisense morpholino oligonucleotide (MO) to block translation of the protein. Dorsally targeted injection of this MO resulted in defects in rostral neural tube closure, similar to the defects observed in Fuz morphants[6] and in *Fuz* mutant mice (Supplementary Information, Fig. Sd, f). Co-injection of *GFP–RSG1* mRNA suppressed the open neural tube phenotype of RSG1 morphants in a dose-dependent manner, demonstrating that the effect of the MO was specific (Supplementary Information, Fig. S2d, g). To examine the function of RSG1 during ciliogenesis, we used *Xenopus* embryonic epidermis, which is a highly tractable and easily imaged *in vivo* model for mucociliary epithelial development[18]. The MO was targeted specifically to the epidermis by ventral injection, thus circumventing the neural tube phenotype. In these morphants, scanning electron microscopy revealed severe defects in ciliogenesis in the epidermal multiciliated cells (Fig. 2a–c). This phenotype was very similar to that of *Fuz* knockdown (Fig. 2d).

RSG1 contains the invariant Ser/Thr residue whose mutation to Asn has been shown in other GTPases to alter the guanine nucleotide binding affinity and to generate a dominant-negative protein (Supplementary Information, Fig. S2c yellow/pink residues). We therefore mutated this residue and expressed high levels of RSG1^{T65N} in *Xenopus* embryos. Overexpression of RSG1^{T65N} resulted in defective ciliogenesis in multiciliated cells of the epidermis, whereas we observed no effect from overexpression of wild-type RSG1 (Fig. 2e, f). These experiments confirm the results of *RSG1* knockdown and suggest that the GTPase activity of RSG1 is essential for ciliogenesis.

Finally, we examined RSG1 subcellular localization by expression of low levels of GFP–RSG1. We observed that it localized strongly to the vicinity of basal bodies in multiciliated cells (Fig. 2g). This localization is probably accurate, as GFP-RSG1 can rescue the phenotype of RSG1 morphants (Supplementary Information, Fig. S2d, g). By contrast, the GFP–RSG1^{T65N} localized only very poorly to basal bodies (Fig. 2h). Together, the results of knockdown, expression of the dominant-negative, and localization of the GFP fusion proteins, suggest a role for the RSG1 GTPase in ciliogenesis. These results are consistent with a role for this protein in mediating Fuz function.

Our bioinformatic approach successfully revealed new aspects of the molecular network in which Fuz functions, so we extended this approach to investigate the cell biological function of the new protein encoded by the *Fuz* gene. We turned to mouseFUNC, a large-scale community effort to systematically predict mouse gene function using the consensus of diverse computational approaches[19]. MouseFUNC predicted a central role in vesicle trafficking for Fuz (Supplementary Information, Fig. S3a). This suggestion was supported by results of iterative BLAST searches (PSIBLAST), which identified modest similarity between Fuz and the yeast vacuolar fusion protein Mon1 (data not shown).

We next used homology modelling[20,21] to predict the structure of the Fuz protein. Using mGENTHREADER (see Supplementary Information Methods), we predicted that the carboxy terminus of the *Xenopus* Fuz protein should fold into a series of five β-sheets flanked by α helices (Fig. 3a, b; Supplementary Information, Fig. S3c, d). This structure, known as a longin-domain[22], is consistent with a vesicle trafficking function for Fuz. Indeed, the longin-domain is present in the structure of SEDL, a subunit of the vesicle-tethering TRAPP complex that is associated with skeletal dysmorphogenesis[23,24]. Moreover, the longin-domain is shared by several other vesicle trafficking proteins, including subunits of the AP clathrin adaptor complexes[25] and the membrane-fusing SNARE proteins, sec22b, VAMP7 and Ytk6p (refs. 22, 26).

These longin-domain containing proteins are all tightly linked to one another in probabilistic networks of human, mouse and yeast genes,

and this node within the gene networks is tightly linked to other core vesicle-trafficking proteins (Supplementary Information, Fig. S4 and Supplementary Information Methods). However, the scale of these linkages was too large to generate easily testable hypotheses. We therefore returned to the physical interactome data, looking this time for relationships between longin-domain containing proteins with structural similarity to the Fuz C terminus. We found that the longin-domain proteins AP2σ, AP1σ and SEDL were all linked by physical associations to the PCP protein Dvl2 (Fig. 3c), which interacts genetically with Fuz[5,6]. More importantly, AP2σ, AP1σ, SEDL and Dvl2 were all linked by physical association to the CaLponin homology and microtubule-associated protein (CLAMP, also called spef1; Fig. 3c), a microtubule-bundling protein that is a known component of cilia and flagella[7,27,28].

As Fuz is essential for ciliogenesis, we examined whether Fuz might have a role in CLAMP localization. In living *Xenopus* embryos, CLAMP–GFP labelled the axonemes of cilia in multiciliated cells (Fig. 3d, left), as has been reported previously for sperm flagella[28]. In addition to the axonemal labelling, however, we also observed an obvious enrichment at the apical tips of cilia (Fig. 3d, left). To test the effect of *Fuz* knockdown, we used targeted injection to generate *in vivo* mosaic epidermis, where control and morphant cells are intermingled. In these mosaics, the morphant cells are indicated specifically by co-injected mRNA encoding histone 2B-RFP (nucRFP; Fig. 3d, inset). In nucRFP-positive Fuz morphant cells, CLAMP–GFP was visible in the shortened and dysmorphic cilia, but the normal accumulation of CLAMP–GFP at the apical tips was entirely absent (Fig. 3d, right).

This role for Fuz in CLAMP localization was of particular interest because we previously found that CLAMP also colocalizes with Dvl2 in the vicinity of the ciliary rootlet[7], which is a known nexus for vesicle trafficking to cilia[7,29,30]. In control embryos, CLAMP–GFP was restricted to the apical cell surface, where it formed a well-defined, linear structure adjacent to the apically docked basal bodies indicated by co-expressed centrin–RFP (Fig. 4a, a′, a′′ and see refs 7, 18). In contrast to controls, the CLAMP–GFP signal in Fuz morphant embryos was present in larger, irregularly shaped foci. *z*-projections revealed that many of these irregular foci were well below the apical cell surface (Fig. 4b, b′, b′′), although centrin–RFP formed an even line at the apical surface of these cells. This result indicates that Fuz, unlike Dvl[6], is not essential for apical docking of basal bodies, but is essential for apical trafficking of CLAMP. The dual localization of CLAMP–GFP at the basal apparatus and at the apical tip is reminiscent of IFT88 and IFT52 in mammalian cells[31], and our data suggest that Fuz is required for accumulation of CLAMP at both sites.

Because the RSG1 GTPase binds to Fuz and is essential for ciliogenesis, we predicted interference with RSG1 function would elicit a similar CLAMP trafficking phenotype. Indeed, in mosaic embryos, nucRFP-positive RSG1 morphant cells had defects in the trafficking of CLAMP–GFP to the apical cell surface, whereas nearby control cells had no such defects (Fig. 4c, d). In addition, expression of $RSG1^{T65N}$ also severely disrupted apical trafficking of CLAMP–GFP, whereas expression of wild-type RSG1 had little effect (Supplementary Information, Fig. S5). Finally, *RSG1* knockdown also eliminated the accumulation of CLAMP–GFP to the apical tips of cilia in multiciliated cells (Fig. 4e).

Our data thus demonstrate that Fuz and RSG1 act to regulate trafficking during ciliogenesis. Because longin-domain proteins participate in many fundamental vesicle trafficking events[22], we next asked whether Fuz might have a broader role in trafficking than is reflected by the phenotype

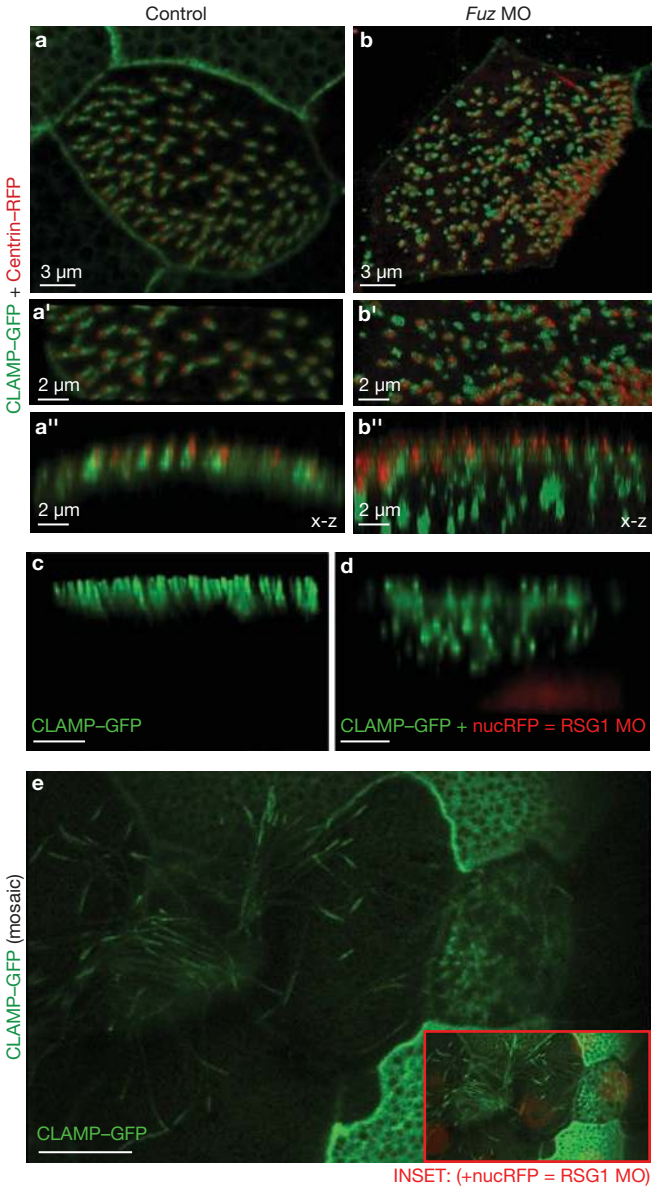

Figure 4 Fuz and RSG1 control trafficking to basal bodies as well as to the tips of cilia. (**a, b**) *Fuz* knockdown disrupts localization of CLAMP–GFP to the ciliary rootlet. Confocal stacks of formaldehyde-fixed *Xenopus* epidermis expressing *centrin–RFP* and *CLAMP–GFP* mRNAs. (**a**) Multiciliated cell in *x-y* view from an uninjected control embryo shows an elongated CLAMP–GFP signal extending from relatively evenly spaced basal bodies (centrin–RFP). (**a′**) Higher magnification view of the *x-y* section from **a**. (**a′′**) *x–z* projection of the stack shown in **a′** shows apical colocalization of centrin–RFP and CLAMP–GFP. (**b**) Ciliated cell in an *x-y* view of the apical surface in a Fuz morphant reveals defects in the spacing of the centrin–RFP signal and defects in elongated CLAMP–GFP signal. Additionally, in many cases, the CLAMP–GFP signal is not faithfully colocalized with the centrin–RFP signal. (**b′**) Higher magnification view of the *x-y* section from **b**. (**b′′**) *x-z*-projection of the stack shown in **b′** reveals apical alignment of the centrin–RFP signal. However, in many cases the CLAMP–GFP signal is below the apical surface in large punctae. (**c–e**) Mosaic imaging of live agarose-embedded embryo. CLAMP–GFP highlights a variety of epidermal structures. RFP–histone 2B (nucRFP) serves as a lineage tracer for MO-injected cells. (**c**, **d**) 3D projections (*x-z*). RSG1 MO (+ nucRFP cells) show defects in normal CLAMP–GFP localization along the apical surface. (**e**) Confocal slice (*x-y*) showing loss of apical-localized CLAMP–GFP to ciliary tips in *RSG1* MO cells (inset shows merge of **e** and more basal slice to show nucRFP signal). Scale bars, 3 μM (**c**, **d**) and 10 μm (**e**).

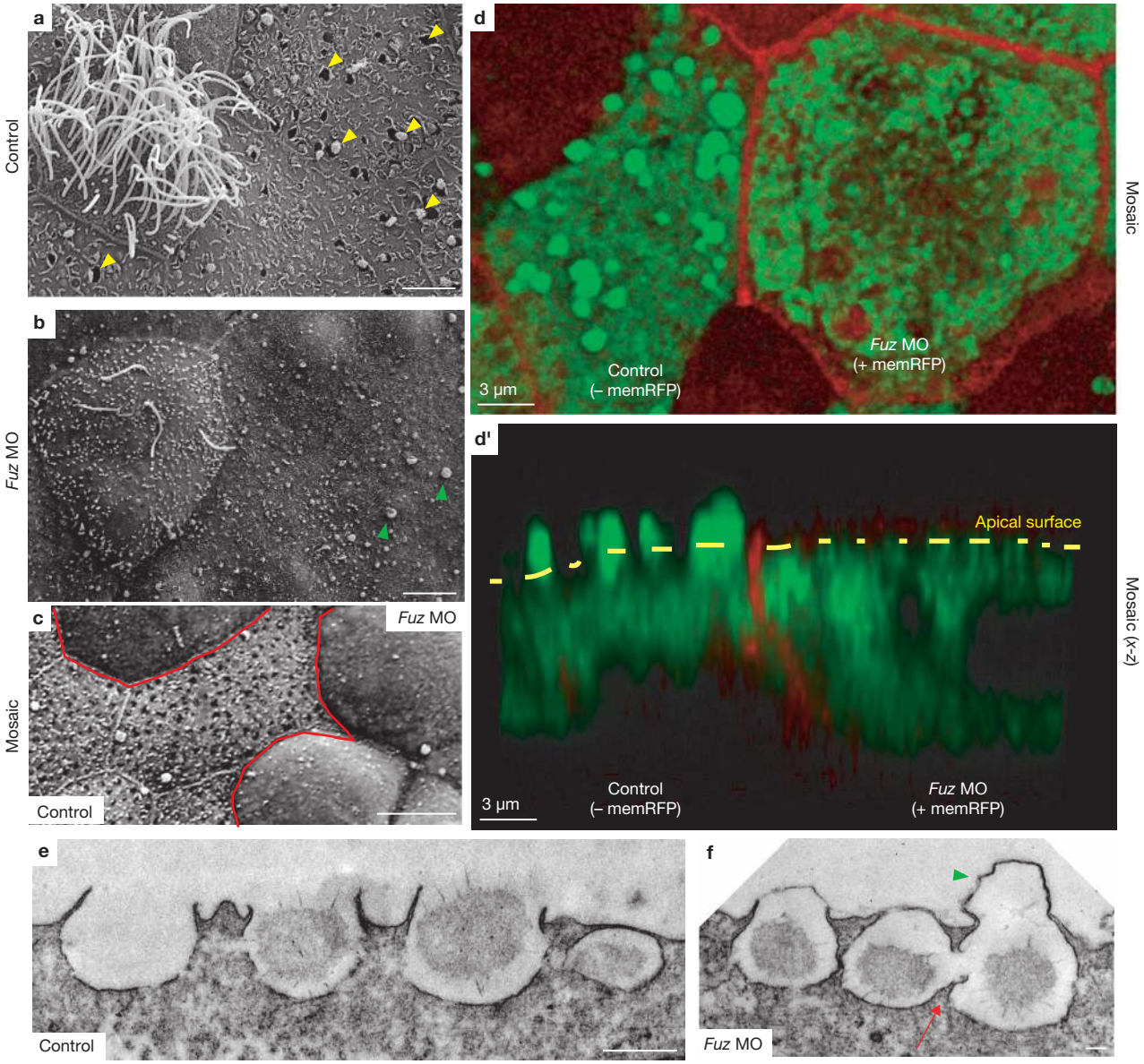

Figure 5 Knockdown of *Fuz* disrupts exocytosis in mucus-secreting cells. (**a**) Wild-type multiciliated cell (Control, left) flanked by secretory cells in *Xenopus* mucociliary epidermis. Control cells have an average of over 90 open exocytic pits per cell. (**b**) Fuz morphants show defects in ciliogenesis in multiciliated cell (left) and failure of exocytosis in mucus-secreting cells (note the absence of exocytic pits indicated by white arrowheads in **a**). Green arrowheads indicate apical membrane blebs (see also panel **f**). In a representative experiment, Fuz morphant cells had fewer than 5 exocytic pits per cell on average (difference from control is significant by the Mann-Whitney U-test; $P<0.0001$). Scale bars, 5 μm (**a**, **b**). (**c**) Mosaic epidermal tissue, with morphant cells outlined in red. Scale bar, 10 μm. (**d**) Confocal section (*x-y*) of mosaic embryo in which membrane–RFP (memRFP, red) mRNA was co-injected with *Fuz* MO and processed for anti-Xeel (Intelectin-2) antibody (green). Cell expressing a high level memRFP (right) lacks apical anti-Xeel antibody staining comparable to the neighbouring cell (right). (**d**′) Confocal projection (*x-z*) of **d** illustrates that the loss of apical anti-Xeel staining (green) in the Fuz morphant cell correlates with apical memRFP expression (right). Scale bars, 3 μm (**d**, **d**′). (**e**, **f**) Transmission electron micrograph of control *Xenopus* epidermis (**e**) shows empty and mucus granule-containing vesicles docked at the apical surface, whereas Fuz morphants (**f**) have a defect of vesicle fusion with the plasma membrane release, as illustrated by large membrane protrusions (green arrows in **b**, **f**). Additionally, frequent homotypic vesicle fusion events were observed in secretory cells of Fuz morphants (red arrow). Scale bars, 500 nm (**e**) and 100nm (**f**).

in multiciliated cells. We examined the mucus-secreting goblet cells that surround the multiciliated cells in the *Xenopus* epidermis[18]. Scanning electron microscopy demonstrated that the apical surface of the goblet cells in controls were decorated with numerous open exocytic vesicles, many of which were actively releasing mucus granules (Fig. 5a). By contrast, open exocytic vesicles were extremely rare and few mucus granules were visible on goblet cells in Fuz morphants (Fig. 5b). We also observed that either knockdown of *RSG1* or overexpression of $RSG1^{T65N}$ elicited defects in exocytosis in mucus-secreting cells (Fig. 2c, f), suggesting that this GTPase is a key effector of Fuz function in multiple cell types.

To confirm the failure of secretion in Fuz morphant goblet cells, we turned again to mosaic epidermis where we examined immunostaining for Intelectin2, a major component of the secreted *Xenopus* epidermal mucus[18,32]. In control cells of these mosaics (indicated by an absence of

membrane–RFP co-injected with the MO), Intelectin2 in exocytosing mucus granules was visible as discrete foci, at or above the apical surface (Fig. 5d, d′). By contrast, Intelectin2 signal was present only below the apical cell surface in neighbouring morphant cells (indicated by the presence of co-injected membrane–RFP in Fig. 5d, d′). The failure of exocytosis in morphant cells in these mosaic epithelia was also confirmed by scanning electron microscopy (Fig. 5c).

The joining of membrane compartments proceeds through discrete steps of transport, tethering and fusion[33]. Our bioinformatic analyses suggested a possible relationship between Fuz and either vesicle tethering or membrane fusion processes (Supplementary Information, Fig. S4); electron microscopy of Fuz morphants supports the latter relationship. Transmission electron microscopy revealed that morphant goblet cells were often decorated by large apical membrane blebs atop putative exocytic vesicles (Fig. 5f, green arrowhead) and this phenotype was obvious with scanning electron microscopy (Fig. 5b, green arrowheads). Such apical membrane blebs were also seen in RSG1 morphants (Fig. 2b, c). Many mucus-filled vesicles in Fuz morphants seemed to be tethered to the apical plasma membrane, although very few had fused (Fig. 5f).

The finding that mucus-filled vesicles in Fuz morphant cells tether to, but fail to fuse with, the apical plasma membrane might suggest a general role for Fuz in governing vesicle fusion. However, secretion in *Xenopus* goblet cells can proceed by compound exocytosis, in which secretory vesicles fuse with one another as they approach the plasma membrane[3,34–36]. We also observed such homotypic fusion of mucus-containing vesicles in Fuz morphants, despite the failure of nearby, seemingly tethered, vesicles to fuse with the plasma membrane (Fig. 5f, red arrow; Supplementary Information, Fig. S6b, c). In some cases, vesicles were observed that had fused to one another, but had not yet tethered to the apical plasma membrane (Supplementary Information, Fig. S6b, arrows). These data demonstrate that Fuz is essential for mediating only a specific subset of membrane fusion events.

The PCP signalling cascade is broadly required for development of vertebrate embryos. However, studies to date have focused on only a small number of the known PCP genes, such as *Dvl* and *Vangl2* (refs 2, 7–9). Here, we have demonstrated that the largely unstudied PCP effector protein Fuz is fundamentally necessary for embryonic development in vertebrates. Our data suggest a central role for Fuz in regulating targeted membrane fusion events, and this cellular function can explain the phenotype of embryos lacking Fuz function.

First, vesicle trafficking to the basal body and within axonemes is essential for ciliogenesis[7,29–31], and the phenotypes observed in *Xenopus* or mouse embryos lacking Fuz function reflect those observed in mice lacking key ciliogenesis factors, such as the BBS or IFT proteins[10,11]. A key role of the cilium in development is thought to be the transduction of Hedgehog signalling[10], so it is relevant that Hedgehog target gene expression is lost in Fuz morphant *Xenopus* embryos[6] and in *Fuz* mutant mice (Fig. 1). Secondly, defective secretion in cells lacking Fuz function may also contribute to the embryonic phenotype. We observed severe skeletal defects in vertebrate embryos lacking Fuz function[6] (Fig. 1); similar skeletal defects are observed in humans or zebrafish with mutations in Sec23A, a subunit of the COPII complex[37,38], and in humans with mutations in the TRAPP complex subunit, SEDL[24].

Our data therefore place Fuz and the interacting GTPase RSG1 at the interface of developmental regulatory systems (such as PCP signalling) and fundamental cell biological processes (such as ciliogenesis and secretion). In combination with the finding that Dvl mediates vesicle association with basal bodies in ciliated cells[7], the data here suggest that coordination of vesicle trafficking might be a unifying mechanism by which PCP signalling can control so many diverse cellular behaviours during embryonic development. □

METHODS

Methods and any associated references are available in the online version of the paper at http://www.nature.com/naturecellbiology/

Note: Supplementary Information is available on the Nature Cell Biology website.

ACKNOWLEDGEMENTS

The ES cell clone for making the *Fuz* mutant mouse was provided by Lexicon Pharmaceuticals. We thank P. Paukstelis for aid with structural modelling, S. Vokes for critical comments on the manuscript, and Wei H. for technical help with histology and immunostaining. Phil Abitua is supported by a Diversity Supplement from the NIH/NIGMS. This work was supported by grants to K.J.L from the Wellcome Trust and the BBSRC; to E.M.M. from the NSF, NIH, Welch Foundation (F-1515), Texas Institute for Drug and Diagnostic Development, and a Packard Fellowship; grants to J.B.W. from the NIH/NIGMS, The March of Dimes, The Burroughs Wellcome Fund, the Sandler Program for Asthma Research, and the Texas Advanced Research Program; and by grants to R.H.F. from the NIH and The Texas A&M Institute for Genomic Medicine.

AUTHOR CONTRIBUTIONS

R.S.G., P.B.A., B.J.W., H.L.S.-R., K.J.L., E.M.M., J.B.W., and R.H.F. designed and interpreted the experiments. R.S.G. performed frog embryo manipulations, construct generation, immunostaining, confocal imaging, structure homology modelling, and protein interactome analysis. P.B.A. performed electron microscopy and EM image analysis. B.J.W. and R.H.F. bred the mice and performed phenotype characterization. B.W.J., H.L.S.-R., K.J.L., R.S.G., and J.B.W. performed mouse immunostaining and imaging. O.B. performed co-immunoprecipiations. G.S.W., I.L., and E.M.M. performed gene network analysis. J.B.W. and R.S.G. assembled figures and wrote the manuscript.

COMPETING INTERESTS

The authors declare that they have no competing financial interest.

Published online at http://www.nature.com/naturecellbiology/
Reprints and permissions information is available online at http://npg.nature.com/reprintsandpermissions/

1. Wallingford, J. B. Planar cell polarity, ciliogenesis and neural tube defects. *Hum. Mol. Genet.* **15,** R227–R234 (2006).
2. Karner, C., Wharton, K. A., Jr. & Carroll, T. J. Planar cell polarity and vertebrate organogenesis. *Semin. Cell Dev. Biol.* **17,** 194–203 (2006).
3. Simons, M. & Mlodzik, M. Planar cell polarity signaling: from fly development to human disease. *Annu. Rev. Genet.* **42,** 517–540 (2008).
4. Collier, S. & Gubb, D. *Drosophila* tissue polarity requires the cell-autonomous activity of the fuzzy gene, which encodes a novel transmembrane protein. *Development* **124,** 4029–4037 (1997).
5. Lee, H. & Adler, P. N. The function of the frizzled pathway in the *Drosophila* wing is dependent on inturned and fuzzy. *Genetics* **160,** 1535–1547 (2002).
6. Park, T. J., Haigo, S. L. & Wallingford, J. B. Ciliogenesis defects in embryos lacking inturned or fuzzy function are associated with failure of planar cell polarity and Hedgehog signaling. *Nature Genet.* **38,** 303–311 (2006).
7. Park, T. J., Mitchell, B. J., Abitua, P. B., Kintner, C. & Wallingford, J. B. Dishevelled controls apical docking and planar polarization of basal bodies in ciliated epithelial cells. *Nature Genet.* **40,** 871–879 (2008).
8. Hamblet, N. S. *et al.* Dishevelled 2 is essential for cardiac outflow tract development, somite segmentation and neural tube closure. *Development* **129,** 5827–5838 (2002).
9. Kibar, Z. *et al.* Ltap, a mammalian homolog of *Drosophila* Strabismus/Van Gogh, is altered in the mouse neural tube mutant Loop-tail. *Nature Genet.* **28,** 251–255 (2001).
10. Huangfu, D. *et al.* Hedgehog signalling in the mouse requires intraflagellar transport proteins. *Nature* **426,** 83–87 (2003).
11. Ross, A. J. *et al.* Disruption of Bardet-Biedl syndrome ciliary proteins perturbs planar cell polarity in vertebrates. *Nature Genet.* **37,** 1135–1140 (2005).
12. Ansley, S. J. *et al.* Basal body dysfunction is a likely cause of pleiotropic Bardet-Biedl syndrome. *Nature* **425,** 628–633 (2003).
13. Sharma, N., Berbari, N. F. & Yoder, B. K. Ciliary dysfunction in developmental abnormalities and diseases. *Curr. Top. Dev. Biol.* **85,** 371–427 (2008).
14. Smith, U. M. *et al.* The transmembrane protein meckelin (MKS3) is mutated in Meckel-Gruber syndrome and the wpk rat. *Nature Genet.* **38,** 191–196 (2006).

15. Beales, P. L. *et al.* IFT80, which encodes a conserved intraflagellar transport protein, is mutated in Jeune asphyxiating thoracic dystrophy. *Nature Genet.* **39,** 727–729 (2007).
16. Takeda, S. *et al.* Left-right asymmetry and kinesin superfamily protein KIF3A: new insights in determination of laterality and mesoderm induction by *kif3A*$^{-/-}$ mice analysis. *J. Cell Biol.* **145,** 825–836 (1999).
17. Rual, J. F. *et al.* Towards a proteome-scale map of the human protein–protein interaction network. *Nature* **437,** 1173–1178 (2005).
18. Hayes, J. M. *et al.* Identification of novel ciliogenesis factors using a new *in vivo* model for mucociliary epithelial development. *Dev. Biol.* **312,** 115–130 (2007).
19. Pena-Castillo, L. *et al.* A critical assessment of *Mus musculus* gene function prediction using integrated genomic evidence. *Genome Biol.* **9** (**Suppl 1),** S2 (2008).
20. Ginalski, K. Comparative modeling for protein structure prediction. *Curr. Opin. Struct. Biol.* **16,** 172–177 (2006).
21. Hagiwara, H., Aoki, T., Ohwada, N. & Fujimoto, T. Development of striated rootlets during ciliogenesis in the human oviduct epithelium. *Cell Tissue Res.* **290,** 39–42 (1997).
22. Rossi, V. *et al.* Longins and their longin domains: regulated SNAREs and multifunctional SNARE regulators. *Trends Biochem. Sci.* **29,** 682–688 (2004).
23. Jang, S. B. *et al.* Crystal structure of SEDL and its implications for a genetic disease spondyloepiphyseal dysplasia tarda. *J. Biol. Chem.* **277,** 49863–49869 (2002).
24. Gedeon, A. K. *et al.* Identification of the gene (SEDL) causing X-linked spondyloepiphyseal dysplasia tarda. *Nature Genet.* **22,** 400–404 (1999).
25. Collins, B. M., McCoy, A. J., Kent, H. M., Evans, P. R. & Owen, D. J. Molecular architecture and functional model of the endocytic AP2 complex. *Cell* **109,** 523–535 (2002).
26. Pryor, P. R. *et al.* Molecular basis for the sorting of the SNARE VAMP7 into endocytic clathrin-coated vesicles by the ArfGAP Hrb. *Cell* **134,** 817–827 (2008).
27. Dougherty, G. W. *et al.* CLAMP, a novel microtubule-associated protein with EB-type calponin homology. *Cell Motil. Cytoskeleton* **62,** 141–156 (2005).
28. Chan, S. W., Fowler, K. J., Choo, K. H. & Kalitsis, P. Spef1, a conserved novel testis protein found in mouse sperm flagella. *Gene* **353,** 189–199 (2005).
29. Fariss, R. N., Molday, R. S., Fisher, S. K. & Matsumoto, B. Evidence from normal and degenerating photoreceptors that two outer segment integral membrane proteins have separate transport pathways. *J. Comp. Neurol.* **387,** 148–156 (1997).
30. Yang, J. & Li, T. The ciliary rootlet interacts with kinesin light chains and may provide a scaffold for kinesin-1 vesicular cargos. *Exp. Cell Res.* **309,** 379–389 (2005).
31. Follit, J. A., Tuft, R. A., Fogarty, K. E. & Pazour, G. J. The intraflagellar transport protein IFT20 is associated with the Golgi complex and is required for cilia assembly. *Mol. Biol. Cell* **17,** 3781–3792 (2006).
32. Nagata, S., Nakanishi, M., Nanba, R. & Fujita, N. Developmental expression of XEEL, a novel molecule of the *Xenopus* oocyte cortical granule lectin family. *Dev. Genes Evol.* **213,** 368–370 (2003).
33. Cai, H., Reinisch, K. & Ferro-Novick, S. Coats, tethers, Rabs, and SNAREs work together to mediate the intracellular destination of a transport vesicle. *Dev. Cell* **12,** 671–682 (2007).
34. Billett, F. S. & Gould, R. P. Fine structural changes in the differentiating epidermis of *Xenopus laevis* embryos. *J. Anat.* **108,** 465–480 (1971).
35. Nachury, M. V. *et al.* A core complex of BBS proteins cooperates with the GTPase Rab8 to promote ciliary membrane biogenesis. *Cell* **129,** 1201–1213 (2007).
36. Sorokin, S. P. Reconstructions of centriole formation and ciliogenesis in mammalian lungs. *J. Cell Sci.* **3,** 207–230 (1968).
37. Boyadjiev, S. A. *et al.* Cranio-lenticulo-sutural dysplasia is caused by a SEC23A mutation leading to abnormal endoplasmic-reticulum-to-Golgi trafficking. *Nature Genet.* **38,** 1192–1197 (2006).
38. Lang, M. R., Lapierre, L. A., Frotscher, M., Goldenring, J. R. & Knapik, E. W. Secretory COPII coat component Sec23a is essential for craniofacial chondrocyte maturation. *Nature Genet.* **38,** 1198–1203 (2006).

METHODS

Generation and genotyping the *Fuz*$^{Gt1(neo)}$ knockout mice. The *Fuz*$^{Gt1(neo)}$ mutant mice were generated by the Texas A&M Institute for Genomic Medicine from targeted ES cells corresponding to clone OST180427 (generated by Lexicon Pharmaceuticals). The gene trapping vector was inserted at the second of 11 exons of the *Fuz* gene in ES cells. This gene trap is predicted to disrupt the transcription of the *Fuz* homologue gene. Specifically, the vector contains a splice acceptor (SA) site followed by a neomycin resistance cassette (NEO). The fused transcript thereby allows antibiotic selection by splicing of the endogenous *Fuz* promoter and upstream exons (E1 and E2) with the NEO cassette. The vector used for producing the *Fuz* homologue ES cells also contains mouse phosphoglycerate kinase (*PGK*) promoter sequence, an exon from Burton's tyrosine kinase (*BTK*), and a splice donor (SD) site. Splicing of this transcript with downstream exons thereby allows identification and localization of the trapping vector within the *Fuz* gene. The *BTK* exon contains stop codons in all three reading frames to prevent translation of downstream fusion transcripts.

Targeted ES cells were selected for blastocyst microinjection into C57BL/6 mice to produce chimaeric mice.To check for germline transmission of the targeted allele, chimaeric males were mated with C57BL/6N females. Heterozygous *Fuz*$^{Gt1(neo)}$ males were then mated with heterozygous *Fuz*$^{Gt1(neo)}$ females to obtain homozygous *Fuz*$^{Gt1(neo)}$ mice. All experimental mice used in this study were of mixed background 129/C57.

Genomic DNA was extracted from the tail samples using the DirectPCR-tail (Viagen Biotech) and used for PCR-genotyping. The product for the wild-type allele was 295 bp long. Primers sequences:

Fuz forward 5′-AGTAGAGGCTCGGAGCCTTTAGG-3′

Fuz reverse 5′-TCACCTAAGCCAGGAACCACTGC-3′

and for the mutant allele (Gt1) was 220 bp. Primers sequence:

Fuz forward 5′-AGTAGAGGCTCGGAGCCTTTAGG-3′ *LTR* reverse 5′-ATAAACCCTCTTGCAGTTGCATC-3′.

Generation of experimental animals. The *Fuz*$^{Gt1(neo)}$ mutant mice were housed in the Institute of Biosciences and Technology Vivarium, which is fully accredited by the AAALAC. The animals were maintained in clear polycarbonate microisolator cages and were allowed free access to food and water (Harlan Teklad Rodent Diet no. 8606, Ralston Purina). The mice were maintained on a 12-h light/dark cycle. Nulligravid heterozygous *Fuz*$^{Gt1(neo)}$ females, 50–70 days of age, were mated overnight with heterozygous *Fuz*$^{Gt1(neo)}$ males and examined for the presence of vaginal plugs the following morning. The onset of gestation was considered to be 10 pm of the previous night, the midpoint of the dark cycle[39]; thus observation of a plug was determined to be embryonic day (E) 0.5. Pregnant females were euthanized by CO_2 asphyxiation on gestation day 18.5, the offspring were collected by caesarian section and evaluated for external malformations. Animal experimentation was approved by the Texas A&M IBT Institutional Animal Care and Use Committee.

Morphological analysis of mouse embryos. Fetuses aged 18.5 days were collected and subjected either to internal organs analysis or bone and cartilage staining. Fetuses were fixed in Bouin's solution and examined for internal organ malformation by Wilson sectioning technique[40]. Some fetuses were fixed in 10% formalin in PBS. Thoracic and abdominal cavities in these fetuses were opened by ventral incision in order to inspect the main organs and their topography *in situ*. From these animals, hearts were obtained and processed for standard histological analysis. The remaining fetuses were subjected to double staining with Alizarin Red S and Alcian blue and examined for skeletal abnormalities[41]. All fetuses were examined and photographed under the dissection stereoscopic microscope (Leica MZ95) with attached digital camera (Leica DFC480 Wetzlar) controlled by Image Pro Plus software (Media Cybernetics)

Prediction of gene function. For MouseFunc-based computational predictions of Fuz function, we used the unified MouseFunc predictions (that is, the composite predictions across MouseFunc participants)[19] for the most probable Gene Ontology biological process and cellular component annotations, ranking likely functions by *P* value. For gene network-based computational predictions of Fuz function, we examined network neighbours of the *Fuz* structural homologues *Sedl*, *AP2σ1*, *AP1σ1*, *sec22*, and *YTK6* in three probabilistic functional networks: a network of yeast genes[42], a network of mouse genes[43] and a network of 470,217 links among 16,375 human genes calculated using the methods described previously for yeast[42] and worm[44] and derived from 22 publicly available genomics datasets including DNA microarray data, protein–protein interactions, genetic interactions, literature mining, comparative genomics and orthologous transfer of gene–gene functional associations from fly, worm and yeast (I.L., E.M.M., manuscript in preparation). For each network, likely association partners of *Fuz* structural homologues were rank-ordered by the sum of the pairwise association scores, corresponding to the naive Bayesian estimate of the probability for the linked genes to participate in the same biological processes as the *Fuz* structural homologues. Additional human protein interaction data were analysed from the BioGRID database[45,46].

Structure modelling. All homology predictions were preformed using the open access PSIPRED protein structure prediction server http://bioinf.cs.ucl.ac.uk/psipred/ as described previously[47,48]. Homology models were built using the Swiss-Model server http://swissmodel.expasy.org/ (ref. 49). All models were rendered using MacPyMol software (http://pymol.sourceforge.net/). The transmembrane domain of Fuz was predicted by MEMSAT3 accessed through the PSIPRED server[47].

***Xenopus* embryo manipulations.** Female adult *Xenopus* were ovulated by injections of human chorionic gonadotropin, and eggs were fertilized *in vitro* and dejellied in 3% cysteine (pH 7.9) and subsequently reared in 0.3× Marc's modified Ringer's (MMR) solution. For microinjections, embryos were placed in a solution of 3% Ficoll in 0.3× MMR solution, injected using forceps and an Oxford universal manipulator, reared in 0.3× MMR solution + Ficoll to stage 9, then washed and reared in 0.3× MMR solution alone. Embryo culture and *in vitro* transcription were performed, and solutions made, according to standard methods[50].

Plasmids and mutagenesis. The following plasmids have been described previously: CLAMP–GFP, CENTRIN–RFP and MIG12–GFP[7,18]; *Fuz* MO (translation blocking 1, 2 and splice blocking) [6]; RSG1 (IMAGE:5571542; Unigene ID: 501682) was purchased from Open Biosystems and cloned into the CS107 vector. RSG1$^{T\to N}$ was generated by Mutagenex, a single point mutant in the 65th codon from ACC to AAC yielding a Thr to Asn mutant. To generate Flag-tagged RSG and RSG1$^{T\to N}$ fusion proteins, GFP tagged RSG and RSG1$^{T\to N}$, and Myc-tagged Fuz, cDNAs were amplified using Vent polymerase (NEB) and subcloned into CS107–Flag-3Stop vector, CS107–GFP vector and CS-MT^{+} vectors, respectively. All constructs were verified by sequencing.

MO and mRNA injections. Capped mRNA was synthesized using mMessage mMachine kits (Ambion). mRNA or antisense MO was injected into two ventral blastomeres at the four-cell stage to target epidermis. MOs were injected at 40 ng per blastomere. Both splice and translation blocking anti-sense oligonucleotide for *Fuz* were described previously[6].

Immunostaining. For immunostaining in *Xenopus*, embryos were fixed in 1× MEMFA (1 h), washed in TBST for 30 min at room temperature, then blocked in 10% FBS and 90% TBST (0.1% Triton X-100 in TBS). Primary antibodies were diluted in 10% FBS and 90%TBST. Antibodies used were monoclonal anti-Xeel (Interlectin-2; 1:1000 dilution) [18]. Primary antibodies were detected with Alexa Fluor-488 goat anti mouse immunoglobulin G (IgG) diluted 1:300 in FBS/TBST solution.

For mice, embryos were fixed overnight at 4°C in 4% paraformaldehyde and dehydrated for storage. For immunohistochemistry, embryos were embedded and sectioned (at 8 μm) according to standard protocols. For detection of acetylated α-tubulin, sections were first de-waxed, rehydrated and treated with proteinase K. Primary antibody incubation (1:25, Sigma cat. no. T7451) was performed overnight at 4°C followed by detection with the Alexa Fluor 594 goat anti-mouse conjugate (1:50, Invitrogen cat. no. A11020). Coverslips were placed on slides stained with Prolong Gold DAPI (Invitrogen cat. no. P36931).

Imaging and image analysis. Immunohistochemistry and mRNA-injected embryos were imaged in TBST on an inverted Zeiss LSM5 Pascal confocal microscope. Confocal images were processed and cropped in Imaris software (BITPLANE scientific solutions) and Adobe Illustrator and Adobe Photoshop for compilation of figures.

DOI: 10.1038/ncb1966

39. Snell, G., Fekete, E. & Hummel, K. The relation of mating, ovulation and the estrus smear in the house mouse to the time of day. *Anat. Rec.* **76,** 30–54 (1948).
40. Wilson, J. Embryological considerations in teratology. in *Teratology: Principles and Techniques.* (ed. J. Wilson) 251–277 (University of Chicago Press, Chicago; 1965).
41. Kimmel, C. A. & Trammel, C. A rapid procedure for routine double staining of cartilage and bone in fetal and adult animals. *Stain Technol.* **56,** 271–273 (1981).
42. Lee, I., Li, Z. & Marcotte, E. M. An improved, bias-reduced probabilistic functional gene network of baker's yeast, *Saccharomyces cerevisiae*. *PLoS ONE* **2,** e988 (2007).
43. Kim, W. K., Krumpelman, C. & Marcotte, E. M. Inferring mouse gene functions from genomic-scale data using a combined functional network/classification strategy. *Genome Biol.* **9** (**Suppl 1),** S5 (2008).
44. Lee, I. *et al.* A single gene network accurately predicts phenotypic effects of gene perturbation in *Caenorhabditis elegans*. *Nature Genet.* **40,** 181–188 (2008).
45. Breitkreutz, B. J. *et al.* The BioGRID Interaction Database: 2008 update. *Nucleic Acids Res.* **36,** D637–D640 (2008).
46. Stark, C. *et al.* BioGRID: a general repository for interaction datasets. *Nucleic Acids Res.* **34,** D535–D539 (2006).
47. McGuffin, L. J., Bryson, K. & Jones, D. T. The PSIPRED protein structure prediction server. *Bioinformatics* **16,** 404–405 (2000).
48. McGuffin, L. J. & Jones, D. T. Improvement of the GenTHREADER method for genomic fold recognition. *Bioinformatics* **19,** 874–881 (2003).
49. Arnold, K., Bordoli, L., Kopp, J. & Schwede, T. The SWISS-MODEL Workspace: A web-based environment for protein structure homology modelling. *Bioinformatics* **22,** 195–201 (2006).
50. Sive, H. L., Grainger, R. M. & Harland, R. M. *Early Development of Xenopus laevis: A Laboratory Manual.* (Cold Spring Harbor Press, NY, 2000).

nature cell biology

DOI: 10.1038/ncb1966

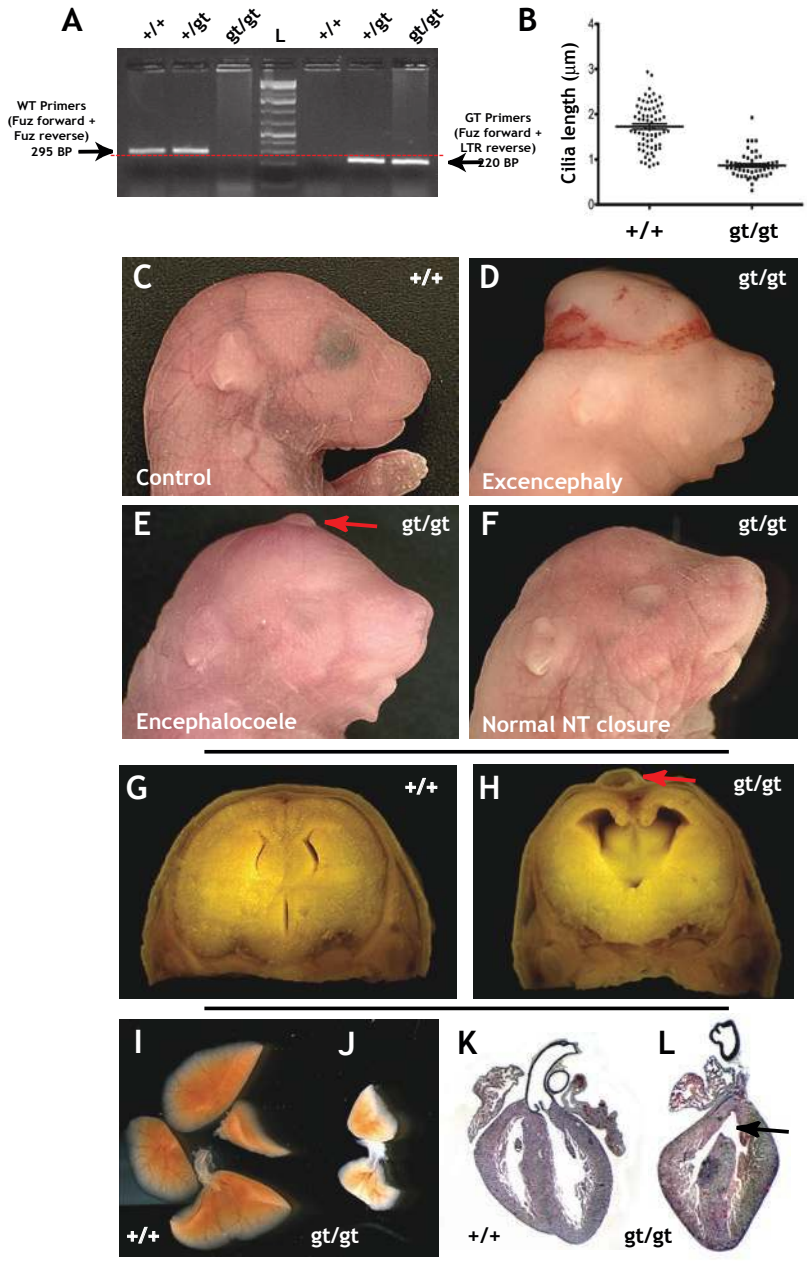

Figure S1 PCR genotyping, cilia length defects, and variably penetrant neural tube closure defects and organogenesis defects in Fuz mutant mice. **(a)** Agarose gel electrophoresis results of $Fuz^{Gt1(neo)}$ knockout mouse PCR genotyping (DNA extracted from tails of fetuses at E18). PCR with primers to detect the wild type allele (Fuz forward & Fuz reverse primers - see Supplemental Methods) produces a 295 bp product, which was detectable in both +/+ and +/gt mice (left). PCR with primers detecting the mutant allele (Fuz forward & LTR reverse - see Supplemental Methods) produces a 220 bp product, which was detected in +/gt and gt/gt mice (right). **(b)** Graph of primary cilia length in chondrocytes of Meckel's cartilage in wild type and Fuz mutant mice, as determined by the length of the acetylated tubulin signal following immunostaining (See Fig. 1G, H). E18.5 mice $Fuz^{gt/gt}$ showing variable NTDs. **(c)** Control mouse. **(d)** $Fuz^{gt/gt}$ mouse displaying excencephaly. **(e)** $Fuz^{gt/gt}$ mouse displaying encephalocoele (red arrow). **(f)** $Fuz^{gt/gt}$ mouse displaying normal neural tube closure (note reduced eyes and jaw). **(g)** Thick section of control brain. **(h)** Thick section of $Fuz^{gt/gt}$ brain from a fetus with an encephalocele (red arrow). **(i, j)** $Fuz^{gt/gt}$ mice display severely hypoplastic lungs. **(k)** Section through control heart. **(l)** Section through $Fuz^{gt/gt}$ heart with ventriculoseptal defect (arrow).

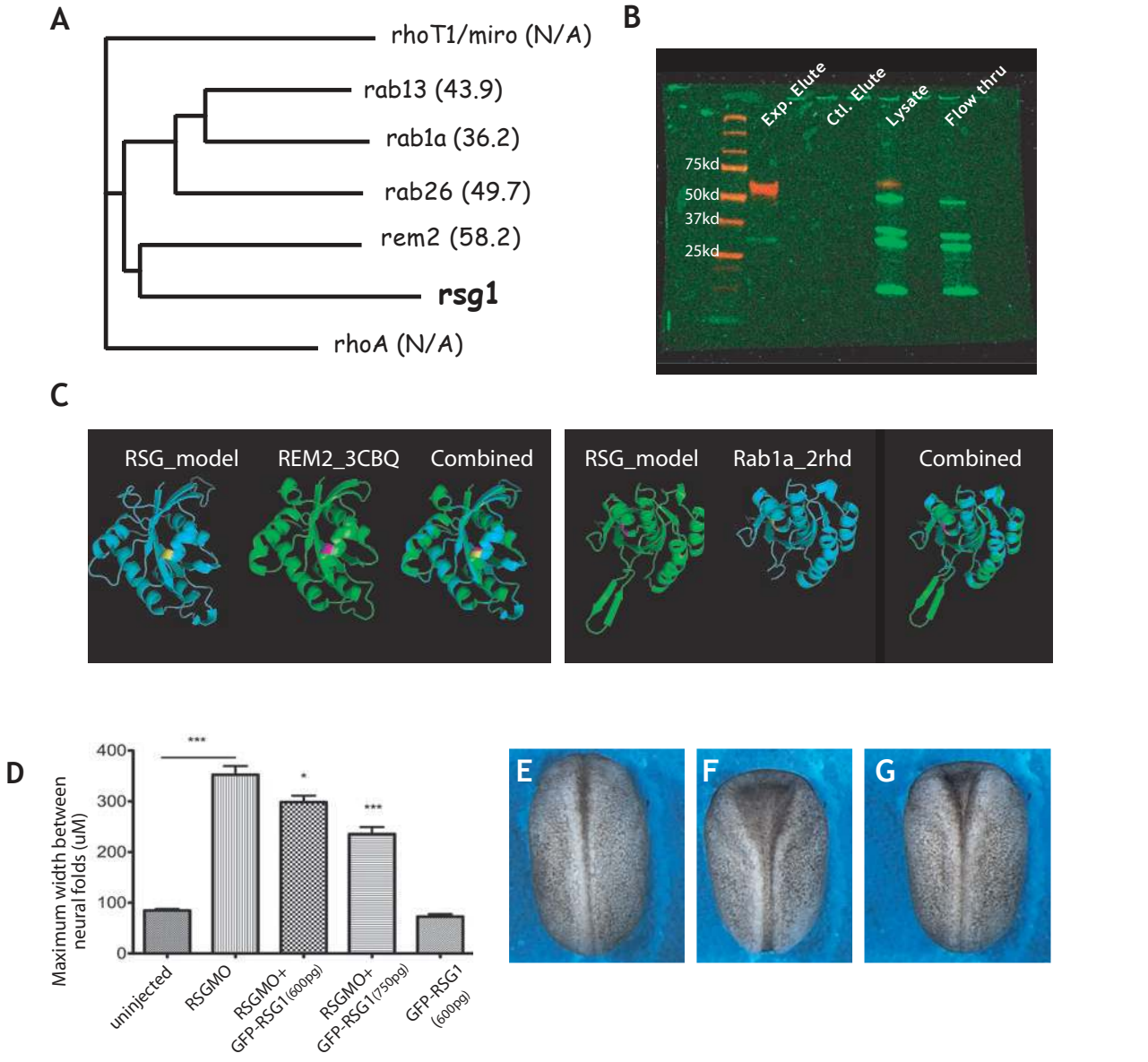

Figure S2 Human chromosome 1 open-reading frame 89 encodes a novel Rab-Similar GTPase (RSG) that is a Fuz interacting protein and dorsally targeted RSG1 MO results in anterior neural tube closure defects that are rescued by co-injection of a GFP-RSG mRNA. **(a)** Neighbor joining tree of human GTPase proteins with RhoT1 and RhoA serving as outgroups. RSG1 forms a clade with REM2 as its closest protein homolog. Parentheses indicate percent amino acid identities to RSG1. **(b)** Co-immunoprecipitation of FLAG-RSG protein (green band at ~27kD in Exp. Elute lane), by pull-down of MYC-FUZ with anti-MYC beads (red band at ~57kD in Exp. Elute lane). Whereas embryo lysates expressing only FLAG-RSG protein exhibit no interactions with anti-MYC beads (Ctl. Elute). Both products are present in raw lysates. **(c, d)** Rendered protein models (Open-Source PyMOL 0.99rc6 software). **(c)** Predicted model of RSG1 (cyan) threaded on the REM2 structure (green) (pdb:3CBQ). **(d)** Predicted model of RSG1 (green) threaded on the Rab1a structure (cyan) (pdb:2RHD). Contrasting colored amino acid (i.e. yellow or magenta) in each structure reflects the location of the conserved threonine residue mutated in our study (T65 in RSG, mutated to N; see main text for discussion). **(d)** RSG morphants exhibit significant defects in anterior neural tube closure compared to uninjected or GFP-RSG1 injected sibling embryos ($P < 0.001$). **(e)** Representative uninjected stage 20 embryo. **(f)** Representative RSG morphant embryo displaying a severe anterior neural tube closure defect. **(g)** Representative GFP-RSG1 (750pg) rescue embryo displaying a subtle but significant decrease in severity of the anterior neural tube defect. * $P < 0.05$ and *** $P < 0.001$ versus RSG morpholino injection embryos or control as indicated by the line. $n = 3$ independent replicate experiments. All P values were analyzed by one-way ANOVA with Bonferoni correction. Data are shown as means ±SEM.

A

GO id	Description	Type	Combined Score	B	C	C*	D	E	F	G	H
GO:0031988	membrane-bound vesicle	CC	0.226	0.00512	0.81	0.897	1	0.0334	0.128	0.00447	0.612
GO:0031982	vesicle	CC	0.22	0.00547	0.798	0.838	1	0.0334	0.183	0.00315	0.603
GO:0031410	cytoplasmic vesicle	CC	0.214	0.00549	0.792	0.867	1	0.000473	0.171	0.00301	0.614
GO:0016023	cytoplasmic membrane-bound vesicle	CC	0.204	0.0133	0.778	0.893	1	0.102	0.14	0.00387	0.624
GO:0006886	intracellular protein transport	BP	0.13	0.0188	0.601	0.735	1	0.0353	0.0407	0.00897	0.56
GO:0008104	protein localization	BP	0.129	0.0123	0.6	0.686	1	0.000426	0.13	0.01	0.559
GO:0016192	vesicle-mediated transport	BP	0.129	0.00592	0.597	0.85	1	0.000457	0.109	0.00676	0.552
GO:0046907	intracellular transport	BP	0.127	0.011	0.595	0.741	1	0.0163	0.0965	0.0105	0.537
GO:0045184	establishment of protein localization	BP	0.126	0.0328	0.593	0.739	1	0.00441	0.0684	0.00913	0.563
GO:0051641	cellular localization	BP	0.125	0.0394	0.591	0.738	1	0.000356	0.168	0.0106	0.543
GO:0015031	protein transport	BP	0.124	0.024	0.587	0.723	1	0.000874	0.0611	0.00901	0.552
GO:0051649	establishment of cellular localization	BP	0.124	0.0403	0.588	0.74	1	0.349	0.0978	0.0106	0.54
GO:0009628	response to abiotic stimulus	BP	0.00729	0.0207	0.0706	0.0171	0.122	0.0352	0.109	0.00847	0.293
GO:0006952	defense response	BP	0.00708	0.0147	0.0687	0.0215	0.00211	0.00137	0.306	0.0101	0.304

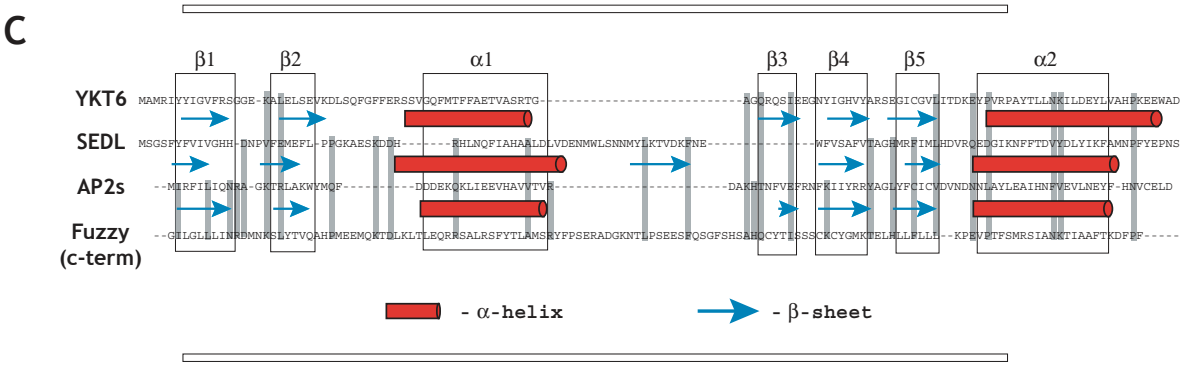

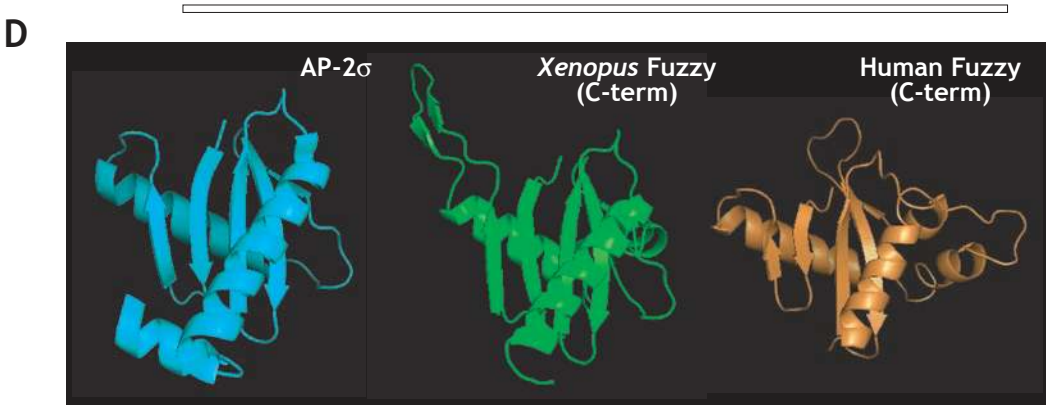

Figure S3 Structure modeling of the Fuz protein. **(a)** MouseFUNC predicts a vesicle trafficking function for Fuz. The description column defines the Gene Ontology descriptors for Fuz function ranked in order of combined score (blue column). Specific Gene Ontology identifiers (GO id's) are listed in the leftmost column. The combined score represents the overall prediction of GO id by all algorithms generated in the MouseFUNC competetion[19]. The columns at right (B-H) are the relative scores for each GO id that were predicted by individual algorithms. The Type column indicates the parent GO hierarchy for the annotations (cc, cellular compartment; bp, biological process). **(b)** The primary sequence of Fuz is predicted to contain a single transmembrane-spanning domain in the N-terminus (MEMSAT3) and a putative longin-domain in the C-terminus (mGENTHREADER). **(c)** Comparison of secondary structures for *Xenopus* Fuz and three longin-domain-containing proteins, Ykt6 (3bw6A0), SEDL (1hgA0), and AP2σ(1vg1S0). The β-sheets and α-helices predicted for *Xenopus* Fuz are indicated by the boxes (see labels above each box). The sheets and helices of the other three proteins are indicated by blue arrows and red barrels, respectively. Critical residues in the Fuz C-terminus, which are conserved in the other proteins, are indicated by the vertical grey bars. **(d)** Rendered protein models of AP-2 (left), and homology threaded model of the C-terminus of *Xenopus* Fuz (middle) and homology-threaded model of the C-terminus of human Fuz (right).

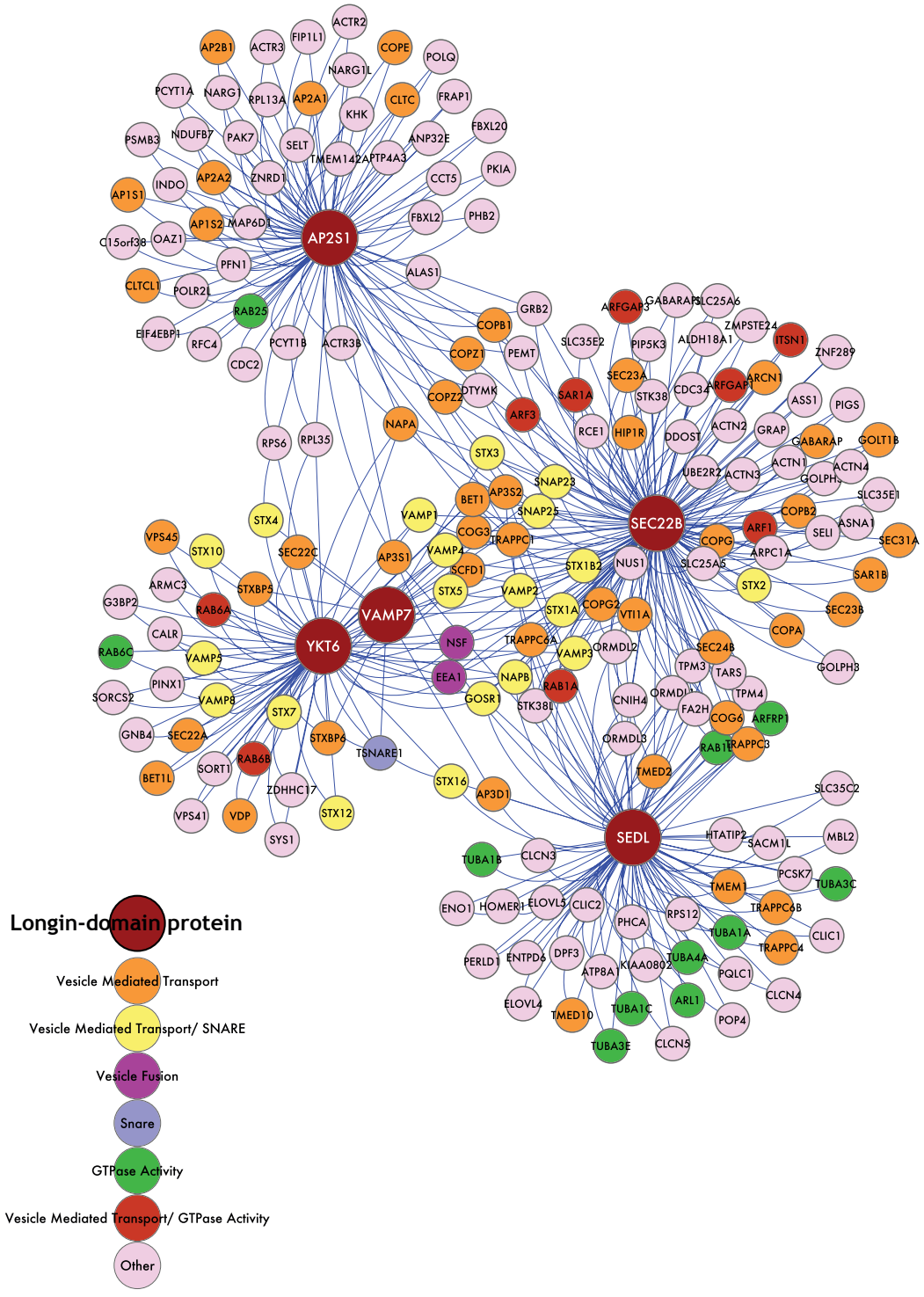

Figure S4 Network diagram of functional interactions between other structurally related Fuz like longin-domain containing proteins SEDL, YKT6, SEC22B, VAMP7 and AP2(PDB id: 1H3Q, 3BW6, 1IFQ, 2VX8 and 1VGL respectively).

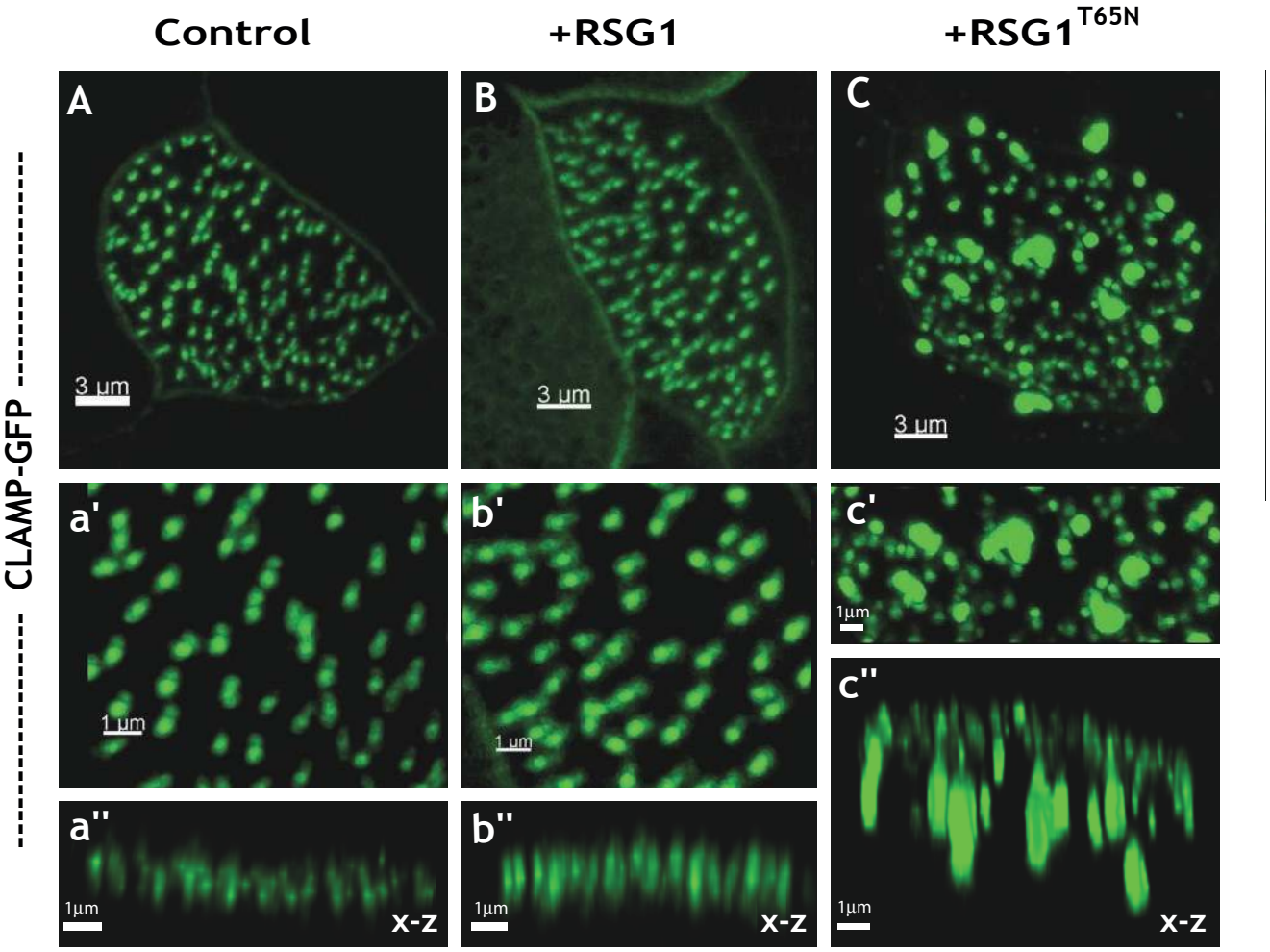

Figure S5 Localization and function of RSG1 in formaldehyde fixed multi-ciliated epidermal cells. **(c)** Multi-ciliated cell view (x-y) of uninjected control embryo exhibits elongated CLAMP-GFP signal. **(c')** Thin x-y section from **[c]**. **(c")** Z-projection of section **[c']** displays apical alignment of CLAMP-GFP. **(d)** Multi-ciliated cell view (x-y) of wild type RSG1 mRNA injected embryo exhibits subtle defects in the elongation of the CLAMP-GFP signal. **(d')** Thin x-y section from **[d]**. **(d")** Z-projection of section **[d']** displays apical alignment of CLAMP-GFP with a subtle defect in the resolution of apical punctae. **(e)** Multi-ciliated cell view (x-y) of RSG1^{T65N} mRNA injected embryo exhibits dramatic defects in the elongation of the CLAMP-GFP signal. **(e')** Thin x-y section from **[e]**. **(e")** Z-projection of section **[e']** displays dramatic loss of the apical alignment as well as aberrant cytoplasmic punctae of CLAMP-GFP signal.

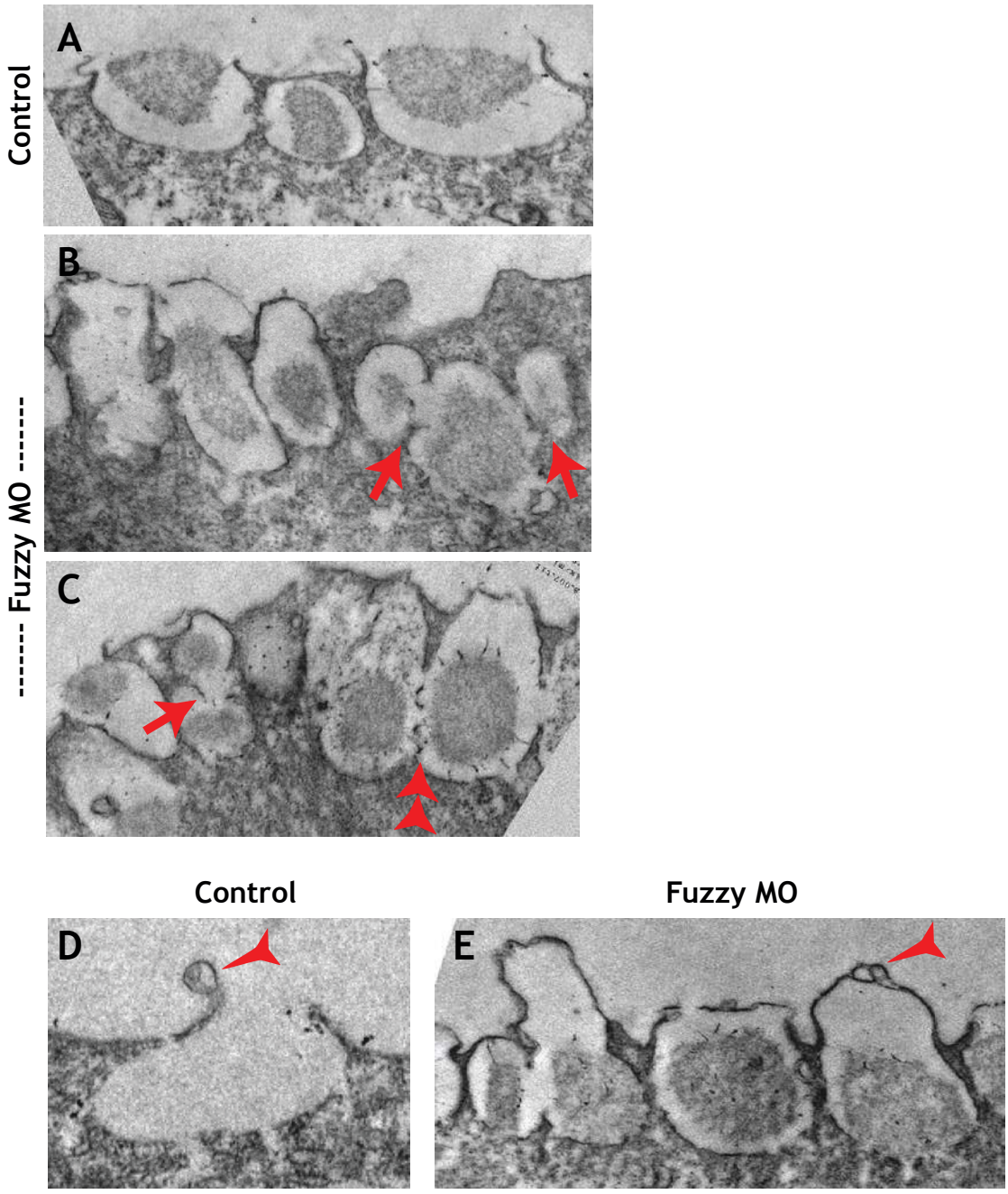

Figure S6 Additional TEM analysis of mucus secreting cells in Fuz morphants. **(a)** Control image showing representative *Xenopus* thin section epidermis. Generally the vesicles display even spacing of vesicles with no lateral mixing. **(b, c)** Fuz morphants display multiple lateral mixing events (red arrows and double red arrowheads **[b, c]**) as well as uneven spacing of the vesicles. **(d)** Wild-type secretory granule. Red arrowhead indicates a membrane signature that maybe indicative of hemifusion. **(e)** Fuz morphant secretory granule. Plasma membrane blebs out significantly, which may indicate a lack of complete fusion. A membrane signature (possibly hemifusion) similar to that observed in in controls cells is present (red arrowhead).